Universidad de La Laguna

Trabajo de Fin de Grado

Dark Matter as Bose-Einstein condensates

Universidad de La Laguna - Facultad de Ciencias

Sección de Física

Autor:

Julio García-Pérez Piñeiro

Supervisor:

Dr. Vicente Delgado Borges

Junio 2021

Resumen

En este trabajo se presenta un modelo para describir la materia oscura basado en los condensados de Bose-Einstein. La materia oscura es un tipo de materia aún desconocida que no interacciona con la radiación electromagnética (como la luz) y que corresponde aproximadamente al 80% de la materia del universo. El modelo más extendido para explicar la materia oscura es el modelo de matería oscura fría (CDM), y aunque presenta resultados exitosos, este modelo se enfrenta a varios problemas que inducen a buscar otro tipo de soluciones. Es aquí donde entra el interés de este trabajo, buscar una alternativa basada en la suposición de que la materia oscura esta compuesta por partículas cuánticas agregadas en condensados de Bose-Einstein.

Contents

1 Introduction and Motivation

En esta primera sección se introducira que es la materia oscura y el interés en su estudio, además razones por las cuales estudiamos el modelo basado en BEC.

In recent decades, a standard model of cosmology has emerged in which the universe consists of 5% ordinary baryonic matter, 27% dark matter, and 68% dark energy. The nature of both matter and dark energy is still unknown, but there is an overwhelming amount of evidence from galactic to cosmological scales that supports the need for both to be part of our universe.

The concept of dark matter arises when studying the rotation curves of galaxies. In early studies it was evident that the amount of matter required to fit the observed plane rotation curve did not coincide with the theoretical curve predicted by Newtonian mechanics. Due to this discrepancy, dark matter (DM) is proposed as an additional (non-luminous) matter that interacts only gravitationally with ordinary matter. Today more evidence of DM is known, some of which we will study deeper in the first section.

The most accepted model for describing our universe today is the Λ-Cold Dark Matter (Λ-CDM) model. In this model, the structure grows hierarchically, with small objects first collapsing under their own gravity and merging into a continuous hierarchy to form objects bigger and more massive. It can be described with only 6 parameters and it parameterizes a large part of the history of the universe. In this theory, dark matter is described as a (perfect) fluid with a very small pressure and speed of sound. Dark energy is parameterized by the cosmological constant (Λ), from which an accelerating expanding universe is deduced.

N-body Simulations performed at $\sim 10kpc$ galactic scales predict that the bound halos surrounding the galaxies must have very characteristic density profiles. These profiles are known as the Navarro-Frenk-White (NFW) profile, which have a well-pronounced central cusp

$$\rho_{NFW}(r) = \frac{\rho_s}{(r/r_s)(1+r/r_s)^2}. \tag{1}$$

where r_s is the radius where the slope of the profile changes and $\rho_s = 4\rho_{NFW}(r_s)$.

Computational simulations have shown that the ΛCDM model is generally consistent with observations of large-scale cosmological structure. However, when we go to smaller scales, we find certain discrepancies between the predictions by the CDM model and the observations. An example of this is the overabundance of small dark matter halos compared to the number of small dwarf galaxies observed orbiting certain galaxies ("the missing satellites problem"). The "cusp-core problem" is also known: almost all CDM simulations show that dark matter halos have a distribution in which the density of dark matter increases abruptly at small radii, while the rotation curves of most of the observed dwarf galaxies suggest they have flat central dark matter density profiles.

These discrepancies have not yet been resolved, which is why new models have been proposed to solve these problems. A very interesting one, and on which this work is based, is to consider dark matter as a Bose-Einstein condensate. Its most recent results are promising.

To learn more about this model, we will introduce the idea of dark matter and its evidences, we will explain conceptually the Bose-Einstein condensates, we will derive its equations describing the dynamical evolution of the condensates (the Gross-Pitaevskii equation). We will derive the density profiles of dark matter halos considering them as Bose-Einstein condensates and finally we will present the results of this model.

2 Dark Matter

En este capítulo se introduciran las evidencias que se han descubierto durante el último siglo que han llevado a introducir hipótesis basadas en materia oscura frente a otras hipótesis (MOND). Y por último se mostraran los problemas a los que se enfrentan los modelos actuales frente a los datos que se obtienen observacionalmente.

2.1 Evidences

The evidence that 90% of the mass of galaxies and clusters is made of dark matter (DM) comes from rotation curves (towards tens of kpc), gravitational lensing (up to 200 kpc) and hot gas in clusters.

2.1.1 Rotation curves

In the 1970s, Ford and Rubin [1] observed that the speeds of objects (stars or gas) orbiting the centers of galaxies, instead of decreasing as a function of distance as expected, remained constant over very large radii leading them to conclude that the rotation curves of galaxies are flat. A plausible explanation for this phenomenon is that the galaxies contain much more mass than can be accounted for by the "visible" stellar objects that reside in the galactic disks, this mass being the one that provides the necessary force to accelerate the orbits. This "non-visible" mass is explained by introducing dark matter.

Rubin and Ford studied more than 60 galaxies and found the same phenomenon. The conclusions of this study have been subsequently confirmed by other independent observations. Normally, the ordinary mass of a galaxy is of the order of 10% of the total, with the remaining 90% being dark matter. This can be seen in Figure 1, where the velocity profile of the galaxy NGC 6503 is shown as a function of the radial distance from the center of the galaxy. However, at the cosmic level the proportions are 80-85% dark matter and 15-20% ordinary matter. The main reason is that most of the ordinary matter is found in intergalactic gas. Although the Rubin and Ford study is considered the first clear evidence of the presence of dark matter halos, Fritz Zwicky was the first astronomer to propose the

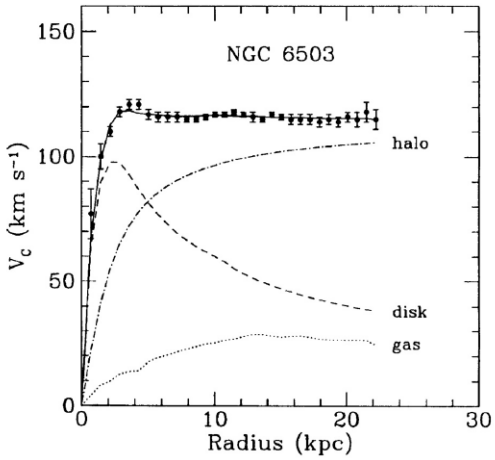

Figure 1: Galactic rotation curve for NGC 6503 showing disk and gas contribution plus the dark matter halo contribution needed to match the data [2].

existence of dark matter based on observational evidence in 1933 [1]. Still, after a study by Rubin and Ford, it was unclear whether dark matter was just ordinary hard-to-detect matter or a new type of unknown matter. There was also the possibility that Newton's law would fail at great distances.

Although they are great evidence, the rotation curves have certain limitations, and that is that you can only look as far as there is light or neutral hydrogen (21 cm), i.e., at distances of tens of kpc. So you can see the beginnings of dark matter halos, but you cannot trace where most of the DM is.

2.1.2 Galaxy clusters

They are clusters of galaxies that contain many galaxies, the mass of the most massive clusters varies between $10^{14} - 10^{15} M_{\odot}$ and the size is around 3 million light years. The composition of these clusters is 10% gas, 1% galaxies, and 90% dark matter. One way to see the halo of dark matter in clusters is through the fact that galaxies and clusters are moving much faster than they would if there were no dark matter, and secondly, the gas is moving so fast that it emits radiation at very high temperature.

Figure 2 illustrates the Coma group. As can be seen, the X-ray image indicates the presence of hot gas, the existence of which in the cluster can only be explained by a large

component of dark matter that provides the potential well to retain the gas.

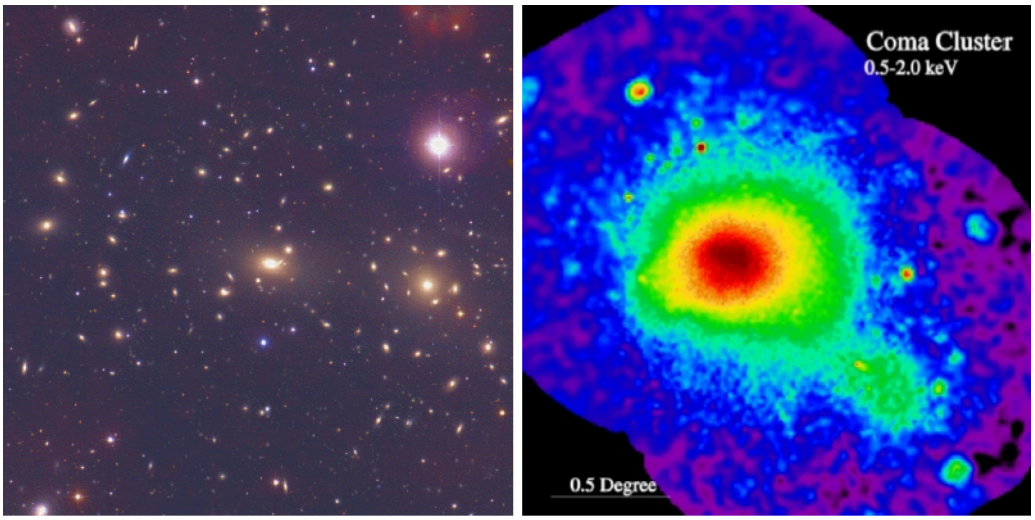

Figure 2: COMA Cluster: without dark matter, the hot gas would evaporate. *Left panel*: optical image. *Right panel*: X-ray image from ROSAT satellite [2].

2.1.3 Gravitacional lensing

Einstein's theory of general relativity predicts that in the presence of gravity, mass and even light bend. Therefore, this effect can be used to determine the existence of mass even when it does not emit light. In the observations of gravitational lensing the sources would be galaxies or quasers and the lenses would be massive objects such as galaxy clusters. The Sloan Digital Sky Survey used faint lenses to conclude that galaxies are even larger and more massive than previously thought, requiring even more dark matter at great distances. This confirms the existence of enormous amounts of dark matter both in galaxies and in galaxy clusters.

2.1.4 CMB Anisotropies

One of the most powerful evidences for the existence of dark matter is found by making cosmological-scale measurements of anisotropies in the cosmic microwave background (CMB). The CMB is a form of electromagnetic radiation discovered in 1965 that fills the entire universe. This is the remnant radiation from the first hot stages of the universe. During these early days at the origin of the universe, photons underwent oscillations that froze just before decoupling from baryonic matter. With a mathematical analysis of these

oscillations, cosmological parameters can be extracted. This is depicted in figure(3). From the analysis of the angular scale of the first peak it is deduced that the geometry is flat (light travels in a straight line), which corresponds to a density of the universe of $\sim 10^{-29} g/cm^3$. From the height of the second peak it is deduced that 5% of the total is ordinary matter, while from the contribution of all the peaks it is found that 26% of the total is dark matter. This reinforces the evidence for dark matter.

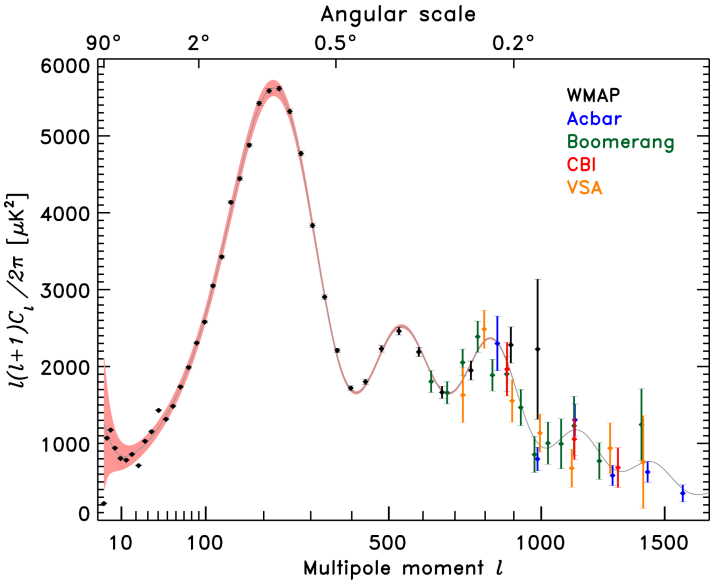

Figure 3: Planck's power spectrum of temperature fluctuations in the cosmic microwave background. Data shown are from WMAP (2006), Acbar (2004) Boomerang (2005), CBI (2004) and VSA (2004).

2.2 Other hypotheses: MOND

In 1983, Milgrom proposed a different idea than the ones now proposed for the explanation of the challenges that had been encountered on a small scale for the explanation of galactic evolution. This proposal, known as modified Newtonian dynamics (MOND), defends the idea of a universe without DM that has a modified force law for small accelerations. MOND says that in the limit of very low accelerations ($a \ll a_0 \sim 1.2 \times 10^{-10} m/s^2$), instead of obeying Newton's second law $F = ma$, the force due to gravity is explained by $F = ma^2/a_0$. With this modification in Newton's second law the observed movements of stars and gas within galaxies could be explained without the need to introduce dark matter.

This line of research has continued to develop and evolve over recent years, with successes and failures in the observations that have been made. At present, the biggest problems MOND faces are CMB anisotropies and gravitational lenses, as they cannot be explained without introducing dark matter.

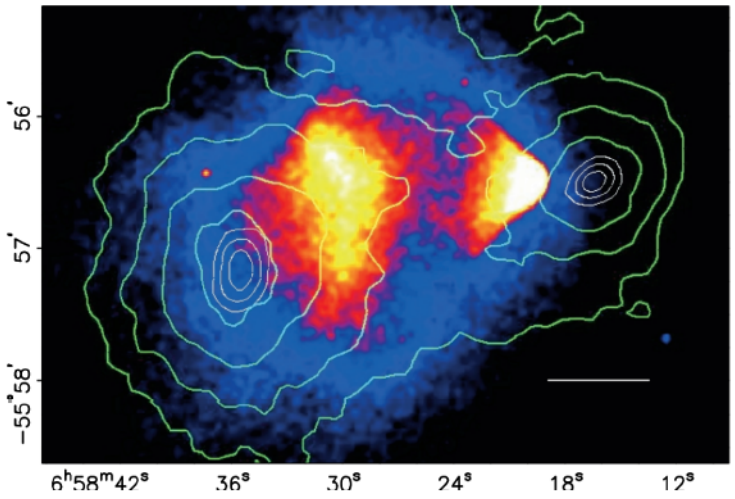

Figure 4: The bullet cluster. The blue color represents dark matter and the red and yellow color is the baryonic matter. The green contours denote the reconstructed gravitational lensing signal, proportional to the projected mass in the system [1].

Figure 4 shows a bullet-shaped galaxy cluster (formed by the collision of two smaller clusters). In the merger of the clusters, the dark matter crossed the collision point without interacting, while the baryonic matter slowed down due to the gravitational interaction that it felt. Theories like MOND cannot predict such a differentiation of these two components of matter.

2.3 Small scale controversies

This section will show how some of the theoretical predictions of the small-scale simulations considering the ΛCDM model are compared with respect to the observations made. The result of this comparison is a series of discrepancies that question the results of the simulations and, in some cases, limitations in the observations. I will present some of these challenges in this section.

2.3.1 Cusp-Core Problem

In the observations made by "The Hi Nearby Galaxy Survey" (THINGS) of dwarf galaxies, quite significant discrepancies have been found between the observations and the simulations carried out using the ΛCDM model. Dwarf galaxies, as well as low surface brightness (LSB) galaxies, are very interesting to study the properties of dark matter because they are cosmic structures where the contribution of dark matter is dominant compared to baryonic matter. When the rotation curves derived from the cusp-shaped distribution of dark matter in CDM halos are compared, it is observed that they increase very slowly. However, using core-like models, dominated by a central core of constant density, these curves are more precisely described. It has also been seen that in dwarf galaxies, the mean value of the logarithmic internal slopes of the mass density profiles is $\alpha = -0.29 \pm 0.07$, while the value of $\alpha = 0.2 \pm 0.2$ is taken for a significantly large sample of LSB galaxies. Knowing that for dark-matter-only simulations the slope is $\alpha = -1.0$, it is observed that the difference in these values is quite relevant.

These problems could be solved by different DM physics, by mechanisms that suppress small-scale subhalo formations, and reduce the central densities of massive subhalos. Later we will see how the Bose-Einstein condensing model can address some of these problems.

2.3.2 Dwarf galaxy problem and too big to fail

The dwarf galaxy problem, also known as the missing satellites problem, basically refers to the discrepancy between the abundance of subhalos predicted by CDM versus the number of satellite galaxies that are known in the Local Group, where the abundance predicted by CDM is greater. Given these problems, the most widely accepted interpretation is that the smallest dark matter halos in the universe are quite inefficient in the formation of stars and other astronomical objects. With the discoveries of new galaxies in the Local Group and the inclusion of the data from the Dark Energy Survey (DES), these discrepancies have been reduced, and it is expected that DES and possible future observations will discover more ultra-faint galaxies, which would reduce even more these discrepancies, although it is still debated whether this would solve the problem. In fact, various studies indicate that satellite galaxies are really lacking in the Local Group, even taking into account our ability

to detect new galaxies.

The study of the missing satellites problem also leads to another challenge, the one too big to fail. When to fit the CDM simulation the visible subhalos of the galaxies are said to be just a set symbolizing the most massive subhalos in the total subhalo distribution, these subhalos must be the most massive ones that the simulation predicts. However, in the simulations we find that the most massive subhalos have central masses significantly large to host observed satellite galaxies. So it is clear that the most massive subhalos must be too large to fail to form galaxies.

Although this has been a problem that has challenged scientists for many years, recent studies ensure that too big to fail is not a problem in the CDM scenario [3].

2.3.3 Regularity in the Face of Diversity

Of the most puzzling aspects of galaxy phenomenology in the context of CDM are the close scale relationships between dynamic and baryonic properties, which hold even for systems dominated by dark matter. The Tully-Fisher baryon relationship (BTFR) is one of the best known examples of this. This relationship presents a close connection between the total baryonic mass of a galaxy and its asymptotic circular velocity:

$$V_f^4 = a_0 G_N M_b \tag{2}$$

where a_0 is the critical acceleration. BTFR is represented in Figure 5, and as can be seen, its slope is different from that predicted by the ΛCDM model, $V_f^3 \propto M_b$, which is represented in dashed lines.

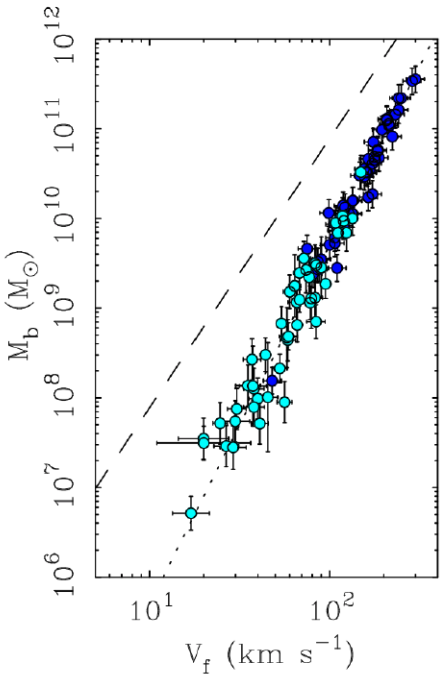

Figure 5: The figure represents BTFR, which shows the relationship between the asymptotic circular velocity of certain galaxies and the baryonic mass. The dark blue points represent star dominated galaxies, and the light blue points gas-dominated ones. The dashed line has slope 3, as expected by the ΛCDM; while the dotted line has slope 4 [4].

The challenge is to understand how there is so much diversity in the shapes of the rotation curves of galaxies compared to those expected by the ΛCDM model, seeing that there are close correlations with the baryonic content.

3 Bose-Einstein Condensates

Se introduce historicamente los condensados de Bose-Einstein

The Bose-Einstein condensate (BEC) is the state of a low-density boson gas at temperatures close to 0K. Normally, in a macroscopic system, composed of numerous particles, there are a large number of quantum states per particle, available for occupation. However, in a BEC an appreciable number of the particles that compose it are in the same quantum state, which is the one with the lowest energy. Therefore, the state of the complete system can be described exactly by the same magnitudes as the quantum state of a single of its component particles, and therefore it is possible to observe coherent quantum properties on a macroscopic scale.

This state of matter was predicted in 1924 by Satyendra Nath Bose and Albert Einstein. In this year, Bose sent a paper to Einstein in which he derived the Planck distribution for blackbody radiation, by statistical means, treating photons as a gas of identical particles. Einstein generalized Bose's work to ideal gases of identical particles with a fixed number of particles. Einstein predicted that from a certain temperature most of the particles would be forced to remain in the lowest energy state. The particles that can condense in the same quantum state are bosons, or what is the same, particles with an integer spin quantum number; since fermions, which have half-integer spin, cannot share the same microstates due to the Pauli exclusion principle (although by forming Cooper pairs, as occurs in superconductivity, fermions can also condense).

In 1995, Bose-Einstein condensation (BEC) was observed for the first time in a series of experiments with rubidium and sodium vapors in which the atoms were confined in magnetic traps, and then cooled to very low temperatures, until the order of fractions of microkelvins. Later, when the confinement trap was turned off, the atoms expanded and images could be obtained with optical methods. The BEC could be observed since a sharp peak was obtained in the velocity distribution below a certain critical temperature (Figure 6). BEC signatures were also found on lithium vapors in that same year [5].

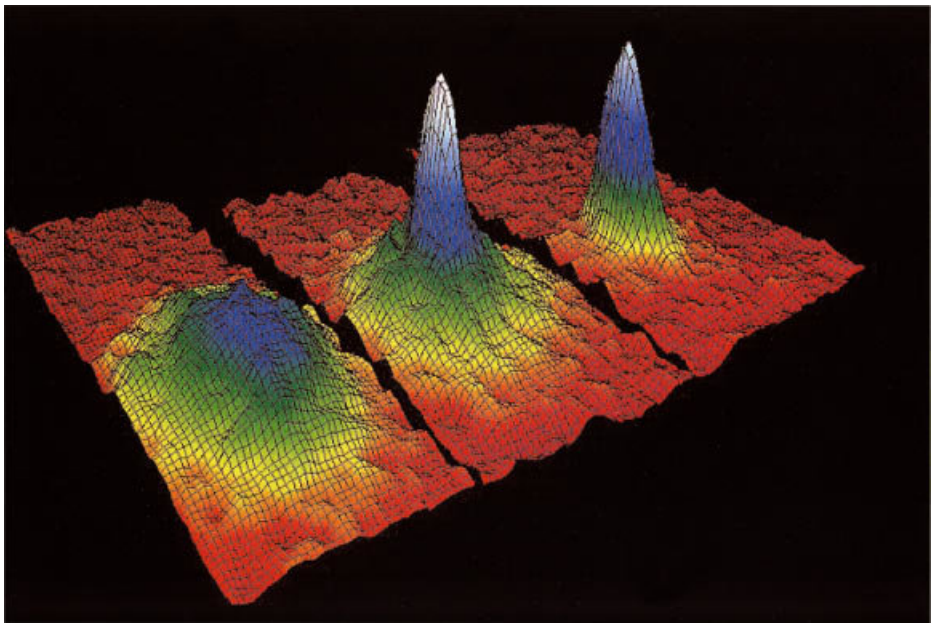

Figure 6: Images of the velocity distribution of rubidium atoms in the experiment by Anderson , taken by means of the expansion method. The left frame corresponds to a gas at a temperature just above condensation; the center frame, just after the appearance of the condensate; the right frame, after further evaporation leaves a sample of nearly pure condensate. The field of view is $200\mu m \times 270\mu m$, and corresponds to the distance the atoms have moved in about $1/20s$. The color corresponds to the number of atoms at each velocity, with red being the fewest and white being the most. From Cornell (1996) [5].

The experiments on the alkalis carried out in 1995 are a milestone in BEC's history, however they were not the first to be carried out in this field. 15 years earlier, attempts were made to condense atomic gases in a series of experiments, where hydrogen atoms were first cooled in a dilution refrigerator, to later be trapped in a magnetic field and then cooled further by evaporation. These experiments came close to obtaining BEC, but were still limited by the recombination of individual atoms to form molecules.

During that time, in the 1980s, techniques such as laser cooling and magneto-optical trapping could be developed in order to cool and trap neutral atoms. These methods are suitable for alkali atoms since their optical transitions can be excited by lasers and also because they have a favorable internal energy level structure for cooling to very low temperatures. Once trapped, their temperature can be further lowered by evaporative cooling. By combining these two methods to cool the alkaline atoms, it has been possible to achieve the

temperatures and densities necessary to observe BEC. It is important to note that under the conditions described, the equilibrium configuration of the system would be the solid phase. So if you want to observe BEC, the system has to be preserved in a metastable gas phase for a long enough time, which is possible because three-body collisions are rare events in cold, dilute gases, so that his life is long enough to carry out the experiments.

4 Derivation of the Gross-Pitaevskii equation

En este capítulo se deriva detalladamente la ecuación de Gross-Pitaevskii en presencia de un potencial externo gravitatorio.

As is well known, there is no analytical solution to the problem of multi-particle systems. In the case of BECs, the number of particles is usually greater than one hundred, so it is necessary to simplify the Hamiltonian that governs the condensate. To achieve this goal, we can estimate the contribution of interactions between particles. Since we work at $T = 0K$, that is, we have the lowest energy, the dispersion of the two particles can be considered as corresponding to the scattering process of the s-wave. In this situation, the scattering is completely characterized by a single parameter, the scattering length a_s. In the cases that we are interested in, this takes a positive value (repulsive interaction between particles). Therefore, any interaction potential can be chosen as long as it leads to the same scattering length of the s-wave that can be measured experimentally, in particular, one of the form $V(\vec{r}_i - \vec{r}_j) = U_0\delta(\vec{r}_i - \vec{r}_j)$.We know that in the Born approximation the scattering length of the s-wave is

$$a_s = \frac{\widetilde{\mu}}{2\pi\hbar^2}\int d\vec{r}_{ij}V(\vec{r}_{ij}) \qquad \vec{r}_{ij} = \vec{r}_i - \vec{r}_j \tag{3}$$

where $\widetilde{\mu}$ is the reduced mass of the two particles in the scattering. Substituting the reduced mass of two bosons $\widetilde{\mu} = m/2$ and the expression chosen above for the potencial $V(\vec{r}_i - \vec{r}_j)$, we find

$$U_0 = \frac{4\pi\hbar^2 a_s}{m} \tag{4}$$

The following is a brief derivation of the stationary Gross-Pitaevskii equation using a variational method in the context of first quantization [6].

4.1 Stationary Gross-Pitaevskii equation from a variational principle

To derive the Gross-Pitaevskii equation, we use the fact that in a BEC all bosons are concentrated in the same quantum state, so we can approximate the total wave function as the symmetric product of identical single-particle wave functions, which leads to a Hartree -Fock ansatz:

$$\psi(\vec{r}_1, \vec{r}_2, ..., \vec{r}_N) = \prod_{i=1}^{N} \phi(\vec{r}_i) \tag{5}$$

As discussed previously, a Bose-Einstein condensate is obtained from a collection of bosons in the ground state at very low temperatures. Therefore, we can ask about the ground state energy and use it to provide us with information about the system. The general Hamiltonian that describes the system is given by

$$\hat{H} = \sum_{i=1}^{N} \left[\frac{\hat{P}_i^2}{2m} + V(\vec{r}_i) \right] + \frac{1}{2} U_0 \sum_{i=1}^{N} \sum_{i \neq j} \delta(\vec{r}_i - \vec{r}_j) \tag{6}$$

where the first term on the right hand side is the kinetic energy of the ith particle, the next term represents the external effects introduced by the trapping potential V and the last term represents the interactions between the N particles.

Given a Hamiltonian $\hat{H}$ and a wave function ψ, we can obtain the energy as follows:

$$E[\psi] = \frac{\langle \psi | \hat{H} | \psi \rangle}{\langle \psi | \psi \rangle} \tag{7}$$

To calculate the energy functional of the system, we can divide it into two contributions, one corresponding to the sum of the energies of a single particle and the other corresponding to the interaction between particles.

The first contribution is given by

$$E_1 = \int d\vec{r}_1 d\vec{r}_2 \cdots d\vec{r}_N \prod_{i=1}^{N} \phi^*(\vec{r}_i) \sum_{i=1}^{N} \left[\frac{P_i^2}{2m} + V(\vec{r}_i) \right] \prod_{i=1}^{N} \phi(\vec{r}_i) = \sum_{i=1}^{N} \int d\vec{r}_i \phi^*(\vec{r}_i) \left(-\frac{\hbar^2}{2m} \nabla_i^2 + V(\vec{r}_i) \right) \phi(\vec{r}_i)$$
$$= N \int d\vec{r} \phi^*(\vec{r}) \left(-\frac{\hbar}{2m} \nabla^2 + V(\vec{r}) \right) \phi(\vec{r}) \tag{8}$$

where we have taken into account that all the terms in the sum are identical.
The second contribution is

$$E_2 = \int d\vec{r}_1 d\vec{r}_2 \cdots d\vec{r}_N \prod_{i=1}^{N} \phi^*(\vec{r}_i) \frac{1}{2} U_0 \sum_{i=1}^{N} \sum_{i \neq j} \delta(\vec{r}_i - \vec{r}_j) \prod_{i=1}^{N} \phi(\vec{r}_i) =$$
$$\frac{1}{2} U_0 \sum_{i=1}^{N} \sum_{i \neq j} \int d\vec{r}_i d\vec{r}_j \phi^*(\vec{r}_i) \phi^*(\vec{r}_j) \delta(\vec{r}_i - \vec{r}_j) \phi(\vec{r}_i) \phi(\vec{r}_j) = \frac{1}{2} U_0 \sum_{i=1}^{N} \sum_{i \neq j} \int d\vec{r}_i |\phi(\vec{r}_i)|^4. \tag{9}$$

Taking into account the form of the sums, this expression can be simplified to

$$E_2 = \frac{N(N-1)}{2} U_0 \int d\vec{r} |\phi(\vec{r})|^4. \tag{10}$$

Since $N \gg 1$ we can approximate $N(N-1) \approx N^2$. So we have that the energy functional $E_N = E_1 + E_2$ is

$$E_N[\phi, \phi^*] = N \int d\vec{r} \phi^*(\vec{r}) \left(-\frac{\hbar^2}{2m} \nabla^2 + V(\vec{r}) \right) \phi(\vec{r}) + \frac{N^2}{2} U_0 \int d\vec{r} |\phi(\vec{r})|^4. \tag{11}$$

We can introduce the energy functional per particle $E = E_N/N$. The functional we have to minimise taking into account the normalisation condition by means of a Lagrange multiplier λ is

$$E'[\phi, \phi^*] = \int d\vec{r} \phi^*(\vec{r}) \left(-\frac{\hbar^2}{2m} \nabla^2 + V(\vec{r}) \right) \phi(\vec{r}) + \frac{N}{2} U_0 \int d\vec{r} |\phi(\vec{r})|^4 - \lambda \int d\vec{r} |\phi(\vec{r})|^2 \equiv \int \mathcal{E}'(\phi^*(\vec{r}), \phi(\vec{r})) d\vec{r} \tag{12}$$

We will use $\phi^*(\vec{r})$ as the "trajectory variable" in phase space for simplicity, which means that the Euler-Lagrange equations reduce to

$$\frac{\partial \mathcal{E}'}{\partial \phi^*} = 0$$

$$\frac{\partial}{\partial \phi^*}\left[\left(-\frac{\hbar^2}{2m}\phi^*(\vec{r})\nabla^2\phi(\vec{r}) + \phi^*(\vec{r})V(\vec{r})\phi(\vec{r})\right) + \frac{N}{2}U_0|\phi(\vec{r})|^4 - \lambda|\phi(\vec{r})|^2\right] = 0 \tag{13}$$

Performing the partial derivative we obtain the following equation

$$\left[-\frac{\hbar^2}{2m}\nabla^2 + V(\vec{r}) + U_0 N|\phi(\vec{r})|^2 - \lambda\right]\phi(\vec{r}) = 0 \tag{14}$$

From this equation we have that the Lagrange multiplier takes the following form

$$\lambda = \langle\phi|\hat{H}|\phi\rangle = \int d\vec{r}\phi^*(\vec{r})\left(-\frac{\hbar^2}{2m}\nabla^2 + V(\vec{r}) + U_0 N|\phi(\vec{r})|^2\right)\phi(\vec{r}) \tag{15}$$

Deriving Eq.(11) with respect to N, we obtain

$$\frac{\partial E_N}{\partial N} = \int d\vec{r}\phi^*(\vec{r})\left(-\frac{\hbar^2}{2m}\nabla^2 + V(\vec{r}) + U_0 N|\phi(\vec{r})|^2\right)\phi(\vec{r}) \tag{16}$$

which is the same expression as that obtained above for λ, and knowing that the chemical potential μ satisfies the relationship $\frac{\partial E_N}{\partial N} = \mu$, we can identify the Lagrange multiplier λ with the chemical potential μ of the condensate. This chemical potential is the amount of energy needed to remove or add one particle to the condensate. With this, we find

$$\left[-\frac{\hbar^2}{2m}\nabla^2 + V(\vec{r}) + U_0 N|\phi(\vec{r})|^2\right]\phi(\vec{r}) = \mu\phi(\vec{r}) \tag{17}$$

which is the stationary Gross-Pitaevskii equation, where it is observed that the stationary states correspond to well-defined values of the chemical potential due to the non-linearity of the Hamiltonian.

4.2 Time-dependent Gross-Pitaevskii equation

Now we are going to derive the time-dependent Gross-Pitaevskii equation using the Dirac-Frenkel variational principle

$$\delta\langle\psi|\left(H - i\hbar\frac{\partial}{\partial t}\right)|\psi\rangle = 0. \tag{18}$$

Dividing Eq.(18) by the number of particles,

$$\delta(E_N/N) - \delta\left[\frac{i\hbar}{N}\langle\psi|\frac{\partial}{\partial t}|\psi\rangle\right] = 0, \tag{19}$$

where the first term is

$$\delta(E_N/N) = \int d\vec{r}\delta\phi^*(\vec{r})\left[-\frac{\hbar^2}{2m}\nabla^2 + V(\vec{r})\right]\phi(\vec{r}) + NU_0\int d\vec{r}\delta\phi^*(\vec{r})|\phi(\vec{r})|^2\phi(\vec{r}) + C.C. \tag{20}$$

And the procedure for calculating the second term is

$$\begin{aligned}\langle\psi|\frac{\partial}{\partial t}|\psi\rangle &= \int d\vec{r}_1\cdots d\vec{r}_N\prod_{i=1}^{N}\phi^*(\vec{r}_i)\frac{\partial}{\partial t}\prod_{i=1}^{N}\phi(\vec{r}_i)\\ &= \int d\vec{r}_1\cdots d\vec{r}_N\phi^*(\vec{r}_1)\cdots\phi^*(\vec{r}_N)\frac{\partial}{\partial t}[\phi(\vec{r}_1)\cdots\phi(\vec{r}_N)]\\ &= \int d\vec{r}_1\phi^*(\vec{r}_1)\frac{\partial\phi(\vec{r}_1)}{\partial t} + \cdots + \int d\vec{r}_N\phi^*(\vec{r}_N)\frac{\partial\phi(\vec{r}_N)}{\partial t},\end{aligned} \tag{21}$$

where we have used the normalization condition. In the last equality all the integrals are identical, so we obtain that

$$\langle\psi|\frac{\partial}{\partial t}|\psi\rangle = N\int d\vec{r}\phi^*(\vec{r})\frac{\partial\phi(\vec{r})}{\partial t} \tag{22}$$

Finally from Eq. (19) we obtain

$$\int d\vec{r}\delta\phi^*(\vec{r})\left[-\frac{\hbar^2}{2m}\nabla^2 + V(\vec{r}) + NU_0|\phi(\vec{r})|^2\right]\phi(\vec{r}) - i\hbar\int d\vec{r}\delta\phi^*(\vec{r})\frac{\partial\phi(\vec{r})}{\partial t} + C.C. = 0 \tag{23}$$

Taking into account the linear independence of the $\delta\phi$ and $\delta\phi^*$ variations we have that,

$$\left(-\frac{\hbar^2}{2m}\nabla^2 + V(\vec{r}) + NU_0|\phi(\vec{r},t)|^2\right)\phi(\vec{r},t) = i\hbar\frac{\partial\phi(\vec{r},t)}{\partial t} \tag{24}$$

which is the time-dependent Gross-Pitaevskii equation.

5 Physical properties of a Bose–Einstein condensate

A partir de la ecuación de Gross-Pitaevskii se expresará la función de onda en forma polar a través de la representación de Madelung, y con ello reescribir la ecuación de Gross-Pitaevskii de forma equivalente en formulación hidrodinámica.

The physical properties of a Bose-Einstein condensate described by the Gross-Pitaevskii equation can be understood more easily using the Madelung transformation [7], rewriting (24) under the form of hydrodynamic equations. For convenience we introduce a new wave function in the form

$$\varphi(\vec{r},t) = \sqrt{N}\phi(\vec{r},t). \tag{25}$$

Then the GPE in terms of φ is

$$\left(-\frac{\hbar^2}{2m}\nabla^2 + V(\vec{r}) + U_0|\varphi(\vec{r},t)|^2\right)\varphi(\vec{r},t) = i\hbar\frac{\partial\varphi(\vec{r},t)}{\partial t} \tag{26}$$

To derive the Madelung equations, we rewrite the wave function φ in the so-called Madelung form

$$\varphi(\vec{r},t) = \sqrt{\rho(\vec{r},t)}e^{iS(\vec{r},t)/\hbar}, \tag{27}$$

where $\rho(\vec{r},t)$ is the particle density, normalized according to $\int d^3\vec{r}\rho = N$, and $S(\vec{r},t)$ has the dimensions of an action .We have

$$\rho(\vec{r},t) = |\varphi(\vec{r},t)|^2. \tag{28}$$

Taking into account the following expressions

$$\frac{\partial}{\partial t}\left(\sqrt{\rho}e^{iS/\hbar}\right) = \frac{1}{2\sqrt{\rho}}\frac{\partial\rho}{\partial t}e^{iS/\hbar} + \sqrt{\rho}\frac{i}{\hbar}e^{iS/\hbar}\frac{\partial S}{\partial t}, \tag{29}$$

$$\nabla^2\left(\sqrt{\rho}e^{iS/\hbar}\right) = \left[\nabla^2\sqrt{\rho} + 2\frac{i}{\hbar}\nabla\sqrt{\rho}\nabla S - \frac{\sqrt{\rho}}{\hbar^2}(\nabla S)^2 + \frac{i}{\hbar}\sqrt{\rho}\nabla^2 S\right]e^{iS/\hbar}, \tag{30}$$

substituting the equation (27) in (26), expanding and then dividing by (27) we obtain

$$Q - \frac{i\hbar}{m\sqrt{\rho}}\nabla\sqrt{\rho}\nabla S + \frac{1}{2m}(\nabla S)^2 - \frac{i\hbar}{2m}\nabla^2 S + V + U_0\rho = \frac{i\hbar}{2\rho}\frac{\partial\rho}{\partial t} - \frac{\partial S}{\partial t}, \tag{31}$$

where

$$Q = -\frac{\hbar^2}{2m}\frac{\nabla^2\sqrt{\rho}}{\sqrt{\rho}} = -\frac{\hbar^2}{4m}\left[\frac{\nabla^2\rho}{\rho} - \frac{1}{2}\frac{(\nabla\rho)^2}{\rho^2}\right] \tag{32}$$

is the quantum potential which takes into account the Heisenberg uncertainty principle. Now we can separate the real and imaginary parts to extract the two Madelung equations. We will start with the imaginary part, but first we introduce the velocity field as

$$\vec{u} = \frac{\nabla S}{m}. \tag{33}$$

Since the velocity is potential, the flow is irrotational: $\nabla \times \vec{u} = \vec{0}$. Taking into account that

$$\nabla^2 S = \nabla(\nabla S) = m\nabla\vec{u}, \tag{34}$$

$$\nabla\sqrt{\rho} = \frac{1}{2\sqrt{\rho}}\nabla\rho, \tag{35}$$

the imaginary part of the equation (31) is

$$\begin{aligned} &\frac{1}{2\rho}(\nabla\rho)\vec{u} + \frac{1}{2}\nabla\vec{u} + \frac{1}{2\rho}\frac{\partial\rho}{\partial t} = 0 \\ &\longrightarrow (\nabla\rho)\vec{u} + \rho\nabla\vec{u} + \frac{\partial\rho}{\partial t} = 0. \end{aligned} \tag{36}$$

Using the properties of the nabla operator,

$$\frac{\partial\rho}{\partial t} + \nabla(\rho\vec{u}) = 0, \tag{37}$$

which is the first Madelung equation (continuity equation).

The real part of (31) is

$$\frac{\partial S}{\partial t} + \frac{(\nabla S)^2}{2m} + V + Q + U_0\rho = 0. \tag{38}$$

Applying the nabla operator and taking into account the expression of the velocity field, we obtain

$$m\frac{\partial \vec{u}}{\partial t} + \frac{1}{2}m\nabla\vec{u}^2 + \nabla V + \nabla Q + \nabla(U_0\rho) = 0, \tag{39}$$

and knowing that $\vec{u}$ is irrotational we can use the property $\nabla(\vec{u}\vec{u}) = 2(\vec{u}\nabla)\vec{u}$, so we finally have the second Madelung equation

$$m\left[\frac{\partial \vec{u}}{\partial t} + (\vec{u}\nabla)\vec{u}\right] + \nabla V + \nabla Q + \nabla(U_0\rho) = 0. \tag{40}$$

6 Static Bose-Einstein condensate

En esta sección se partira de las ecuaciónes de Madelung y se considerará que el condensado es un condensado estático ideal y únicamente sometido a la interacción gravitatoria. Posteriormente se resolvera la ecuación de Helmholtz obtenida para obtener la densidad de masa del condensado.

In the present case we are going to consider an ideal static condensate, $\vec{u} \equiv \vec{0}$. Taking this into account, from Eq. (40) we obtain

$$Q + V + U_0\rho = cte \tag{41}$$

and applying the nabla operator two times on both sides of the equation we have

$$\nabla^2(Q + U_0\rho) + \nabla^2(V) = 0. \tag{42}$$

In our case, the system is in the presence of a gravitational field $V(\vec{r}) = V_g(\vec{r}) = m\Phi(\vec{r})$. The gravitational potential satisfies the Poisson equation.

$$\nabla^2\Phi = 4\pi G\rho_m, \tag{43}$$

where G is the gravitational constant and ρ_m is the mass density of the condensate.

In the Thomas-Fermi regime, when the number of particles in the gravitationally bound Bose-Einstein condensate is large enough, the quantum pressure term Q has a negligible contribution. When the number of particles becomes infinite, the Thomas-Fermi approximation is exact. Taking this into account, Eq.(42) becomes

$$\nabla^2(U_0\rho) + \nabla^2 V_g = 0, \tag{44}$$

Using the Poisson equation and knowing that $\rho_m = m\rho$,

$$\nabla^2\left(U_0\frac{\rho_m}{m}\right)+m4\pi G\rho_m=0$$
$$\frac{U_0}{m}\nabla^2\rho_m+m4\pi G\rho_m=0. \tag{45}$$

We can see that the mass density can be described by a Helmholtz equation,

$$\nabla^2\rho_m+\frac{4\pi Gm^2}{U_0}\rho_m=0. \tag{46}$$

Taking into account the stationary condition in the first Madelung equation (37), it can be seen that the mass density has no temporal dependence, only radial dependence, $\rho_m(\vec{r},t)=\rho_m(\vec{r})$. Defining $k^2=\frac{4\pi Gm^2}{U_0}$, we have

$$\nabla^2\rho_m+k^2\rho_m=0. \tag{47}$$

To solve this equation, we will start by expressing the Laplacian in spherical coordinates

$$\left[\frac{1}{r^2}\frac{\partial}{\partial r}\left(r^2\frac{\partial}{\partial r}\right)+\frac{1}{r^2sin\theta}\frac{\partial}{\partial\theta}\left(sin\theta\frac{\partial}{\partial\theta}\right)+\frac{1}{r^2sin^2\theta}\frac{\partial^2}{\partial\phi^2}\right]\rho_m(\vec{r})+k^2\rho_m(\vec{r})=0, \tag{48}$$

that can be rewritten as

$$\left[\frac{1}{r^2}\frac{\partial}{\partial r}\left(r^2\frac{\partial}{\partial r}\right)-\frac{\vec{L}^2}{\hbar^2r^2}\right]\rho_m(\vec{r})+k^2\rho_m(\vec{r})=0 \tag{49}$$

taking into account that the square of the angular momentum operator is given by

$$\vec{L}^2=-\hbar^2\left[\frac{1}{sin\theta}\frac{\partial}{\partial\theta}\left(sin\theta\frac{\partial}{\partial\theta}\right)+\frac{1}{sin^2\theta}\frac{\partial^2}{\partial\phi^2}\right]. \tag{50}$$

To obtain an equation formally analogous to Schrödinger's equation of a free particle [8], we multiply by the factor $-\hbar^2/2m$,

$$\left[-\frac{\hbar^2}{2m}\frac{1}{r^2}\frac{\partial}{\partial r}\left(r^2\frac{\partial}{\partial r}\right)+\frac{\vec{L}^2}{2mr^2}\right]\rho_m(\vec{r})=\frac{\hbar^2k^2}{2m}\rho_m(\vec{r}). \tag{51}$$

In the interest of simplification of the notation and avoid confusion we will use, for the

time being, the expression of the mass density as $\rho_m(\vec{r}) \equiv \rho(\vec{r})$.

To simplify the solution of this equation, it is important to remember that the operators L_x, L_y, L_z and $\vec{L}^2$ do not operate on the radial variable r. Naming the operator in the square brackets of Eq.(51) as F, we have

$$\left[F\,,\, \vec{L} \right] = \left[F\,,\, \vec{L}^2 \right] = 0. \tag{52}$$

Taking into account that the operators L_x, L_y and L_z do not commute among themselves, it is easy to see that one can take as a set of operators that commute F, $\vec{L}^2$ and any one of L_x, L_y and L_z. If F, $\vec{L}^2$ and L_z are taken as a set, it follows that one can find simultaneous eigenfunctions of these three operators, or in other words, obtain solutions of Eq.(51) that are also eigenfunctions of $\vec{L}^2$ and L_z. Knowing that the spherical harmonics $Y_{lm}(\theta, \phi)$ are eigenfunctions of $\vec{L}^2$ and L_z we will look for solutions of the equation that have the separable form

$$\rho_{klm}(\vec{r}) = R_{klm}(\vec{r}) Y_{lm}(\theta, \phi). \tag{53}$$

Inserting this into the Eq.(51) and knowing that $\vec{L}^2 Y_{lm}(\theta, \phi) = l(l+1)\hbar^2 Y_{lm}(\theta, \phi)$, we obtain for the radial function the differential equation

$$\left[-\frac{\hbar^2}{2m} \left(\frac{d^2}{dr^2} + \frac{2}{r}\frac{d}{dr} \right) + \frac{l(l+1)\hbar^2}{2mr^2} \right] R_{kl}(r) = \frac{\hbar^2 k^2}{2m} R_{kl}(r). \tag{54}$$

It can be observed that the magnetic quantum number m does not appear in this equation, so the radial function is independent of this quantum number. Introducing a new radial function $u_{kl}(r) = r R_{kl}(r)$, we have that

$$-\frac{\hbar^2}{2m}\frac{d^2}{dr^2} u_{kl}(r) + V_{eff}(r) u_{kl}(r) = \frac{\hbar^2 k^2}{2m} = u_{kl}(r), \tag{55}$$

where

$$V_{eff}(r) = \frac{l(l+1)\hbar^2}{2mr^2} \tag{56}$$

Eq.(55) is only meaningful for positive values of r, and must be complemented with a

boundary condition at $r = 0$. We will impose that the radial function $R_{kl}(r)$ is finite at the origin, and since $R_{kl}(r) = u_{kl}(r)/r$, it implies that

$$u_{kl}(0) = 0. \tag{57}$$

In this paper we will focus on solutions for $l = 0$, so $V_{eff}(r) = 0$. The Eq.(55) reduces to

$$\left[\frac{d^2}{dr^2} + k^2\right] u_{k0}(r) = 0. \tag{58}$$

Knowing the boundary condition (57), the solution to this equation has the following form,

$$u_{k0}(r) = Asin(kr). \tag{59}$$

Knowing $Y_{00}(\theta, \phi) = 1/\sqrt{4\pi}$ and Eq.(59), substituting both expressions in (53), we obtain for the condensate mass density $\rho_{k00}(\vec{r}) \equiv \rho_{DM}(r)$,

$$\rho_{DM}(r) = \rho_{DM}^{(c)} \frac{sin\, kr}{kr} \tag{60}$$

where $\rho_{DM}^{(c)}$ is the central density of the condensate, $\rho_{DM}^{(c)} = \rho_{DM}(0)$.

7 Dark Matter as Bose-Einstein condensate

Una vez caracterizado el perfil de densidad de masa con las condiciones impuestas, se extraerá las características más significativas de los halos de materia oscura de las galaxias.

Having characterized the density distribution of the Bose-Einstein condensate of dark matter $\rho_{DM}(r)$, we can now deduce other properties. Let's start with the mass profile of the dark condensed galactic halo. To do this, starting from $dm = \rho dV$ and assuming spherical symmetry we have that

$$dm = 4\pi\rho(r)r^2dr, \tag{61}$$

So in our case the mass will be

$$m_{DM}(r) = 4\pi \int_0^r \rho_{DM}(r')r^{2\prime}dr' = \frac{4\pi\rho_{DM}^{(c)}}{k} \int_0^r sin(kr')r'dr'. \tag{62}$$

To solve the integral we use the method of integration by parts

$$\int_0^r sin(kr')r'dr' = \left[-\frac{r'cos(kr')}{k}\right]_0^r + \int_0^r \frac{cos(kr')}{k}dr' = -\frac{rcos(kr)}{k} + \frac{sin(kr)}{k^2} \tag{63}$$

So we finally get that

$$m_{DM}(r) = \frac{4\pi\rho_{DM}^{(c)}}{k^2} r \left[\frac{sin(kr)}{kr} - cos(kr)\right] \tag{64}$$

To calculate the radius of the condensate R we start from the condition of $\rho_{DM}(R) = 0$, so from the equation (60) we deduce that $kR = \pi$. Knowing the shape of k and U_0 we arrive at

$$R_{DM} = \frac{\pi}{k} = \pi\sqrt{\frac{\hbar^2 a_s}{Gm^3}}. \tag{65}$$

We know that the velocity of astronomical objects moving in circular orbits of radius r around a mass M satisfies the following equation

$$v = \sqrt{\frac{GM(r)}{r}}, \tag{66}$$

in our case

$$v_{tg}^2(r) = \frac{Gm_{DM}(r)}{r} \tag{67}$$

substituting the equation (64)

$$v_{tg}^2(r) = \frac{4\pi G\rho_{DM}^{(c)}}{k^2}\left[\frac{sin(kr)}{kr} - cos(kr)\right]. \tag{68}$$

When $r \longrightarrow 0$ we have that $v_{tg}^2(r) \longrightarrow 0$. The total mass of the condensate using Eq.(64) and the relation $kR = \pi$ is

$$\begin{aligned} M_{DM} = m_{DM}(R_{DM}) &= \frac{4\pi\rho_{DM}^{(c)}}{k^2}R_{DM}\left[\frac{sin(kR_{DM})}{kR_{DM}} - cos(kR_{DM})\right] \\ &= \frac{4R_{DM}^3\rho_{DM}^{(c)}}{\pi}\left[\frac{sin(\pi)}{\pi} - cos(\pi)\right] = \frac{4R_{DM}^3\rho_{DM}^{(c)}}{\pi}. \end{aligned} \tag{69}$$

So the mean value of the density of the condensate will be

$$\langle\rho\rangle = \frac{M_{DM}}{V} = \frac{4R_{DM}^3\rho_{DM}^{(c)}/\pi}{(4/3)\pi R_{DM}^3} = \frac{3\rho_{DM}^{(c)}}{\pi^2}. \tag{70}$$

We can represent the tangential velocity as

$$v_{tg}^2(r) = \frac{GM_{DM}}{R_{DM}}\left[\frac{sin(\pi r/R_{DM})}{\pi r/R_{DM}} - cos\left(\frac{\pi r}{R_{DM}}\right)\right]. \tag{71}$$

When $r > R_{DM}$ the standard Keplerian law is recovered, The mass of the particle in the condensate can be obtained from the radius of the dark matter halo as

$$m = \left(\frac{\pi^2\hbar^2 a}{GR_{DM}^2}\right)^{1/3} \approx 6.73 \times 10^{-2}[a(fm)]^{1/3}[R_{DM}(kpc)]^{-2/3}\, eV \tag{72}$$

Using $a \approx 1\, fm$ and $R_{DM} \approx 10\, kpc$, the mass will be on the order of $m \approx 14\, eV$. For values of $a \approx 10^6\, fm$, corresponding to the values of a observed in terrestrial laboratory experiments, $m \approx 1.44\, eV$. The limit obtained for the mass of the condensate particle from cosmological considerations is $m < 1.87\, eV$, so the values observed are consistent with this limit.

8 Properties of galaxies in the BEC model

En esta sección se comprobará el modelo descrito con los datos observacionales de siete galaxias extraidas de la basa de datos SPARC. Se comparará los perfiles de velocidad de rotación del modelo propuesto con el modelo CDM, así como los perfiles de densidad de los halos de materia oscura.

The following galaxies have been chosen for our study, DDO154, F563-V2, F583-4, UGC01281, UGC04278, UGC07524, UGC07608. Its properties will be analyzed within the framework of the Bose-Einstein condensate model that we have introduced in the previous sections, and we will compare it with the CDM model. This study has been previously performed in references [9] and [10]. The selected galaxies have been extracted from SPARC survey [11] and their interest is because they have high resolution rotation curves and because they are composed mostly of dark matter. To compare the BEC and CDM models, we will first analyze the behavior of the rotation curves, using the predictions of Eq.(68) and Eq.(1) with the observed rotation curves. With this we can determine the free parameters of the equations. Finally, we will obtain the dark matter density profiles of the galaxies for both models.

8.1 Rotational velocity profiles of the galaxies

In this study, we start by comparing the BEC dark matter halo model with the observational data from the rotation curves of galaxies, and also with the rotation speed given by the NFW profile. From Eq. (1) We obtain that

$$V_{NFW}(r) = \sqrt{4\pi G\rho_s r_s^3}\sqrt{\frac{1}{r}\left[ln\left(1+\frac{r}{r_s}\right) - \frac{(r/r_s)}{1+r/r_s}\right]}. \tag{73}$$

We can obtain the observable velocities at different radii of the galaxies from the SPARC database. In this database we also find the contributions to the observable velocity of gas, bulge, and disk. So, knowing that the speeds are not additive, but the masses and $V^2 \propto M$, we can obtain the contribution of dark matter as follows,

$$V_{DM} = \sqrt{V^2 - |V_{gas}|V_{gas} - \Upsilon_{disk}|V_{disk}|V_{disk} - \Upsilon_{bul}|V_{bul}|V_{bul}}, \tag{74}$$

but taking into account that in all the galaxies that have been selected for this study $V_{bul} = 0$, we have that

$$V_{DM} = \sqrt{V^2 - |V_{gas}|V_{gas} - \Upsilon_{disk}|V_{disk}|V_{disk}} \tag{75}$$

As explained in [11], it is necessary to use absolute values because the gas velocity can be negative in more internal regions. This happens when the gas distribution has a considerable central depression and the material in the inner regions exerts a lower gravitational force than in the outer regions. The value of Υ_{disk} used is 0.5, which is a fair value according to [11].

Figure 7 shows the rotation curves predicted by the BEC model (solid curve) and the NFW profile (dashed curve), together with the observational data of the eight galaxies.

The values of the free parameters obtained by fitting the Bose-Einstein condensate (radius and central density) with the observational results are presented in table 1.

Galaxy	R (kpc)	$\rho_{DM}^{(c)}\,(10^{-24}\,gm/cm^3)$
DDO 154	5.1	0.93
F 563-V2	6.34	4.9
F 583-4	6.91	0.85
UGC 01281	4.87	1.34
UGC 04278	8.12	1.14
UGC 07524	8.16	0.91
UGC 07608	4.9	1.89

Table 1: Radii and central densities of the galaxies obtained by fitting the BEC model.

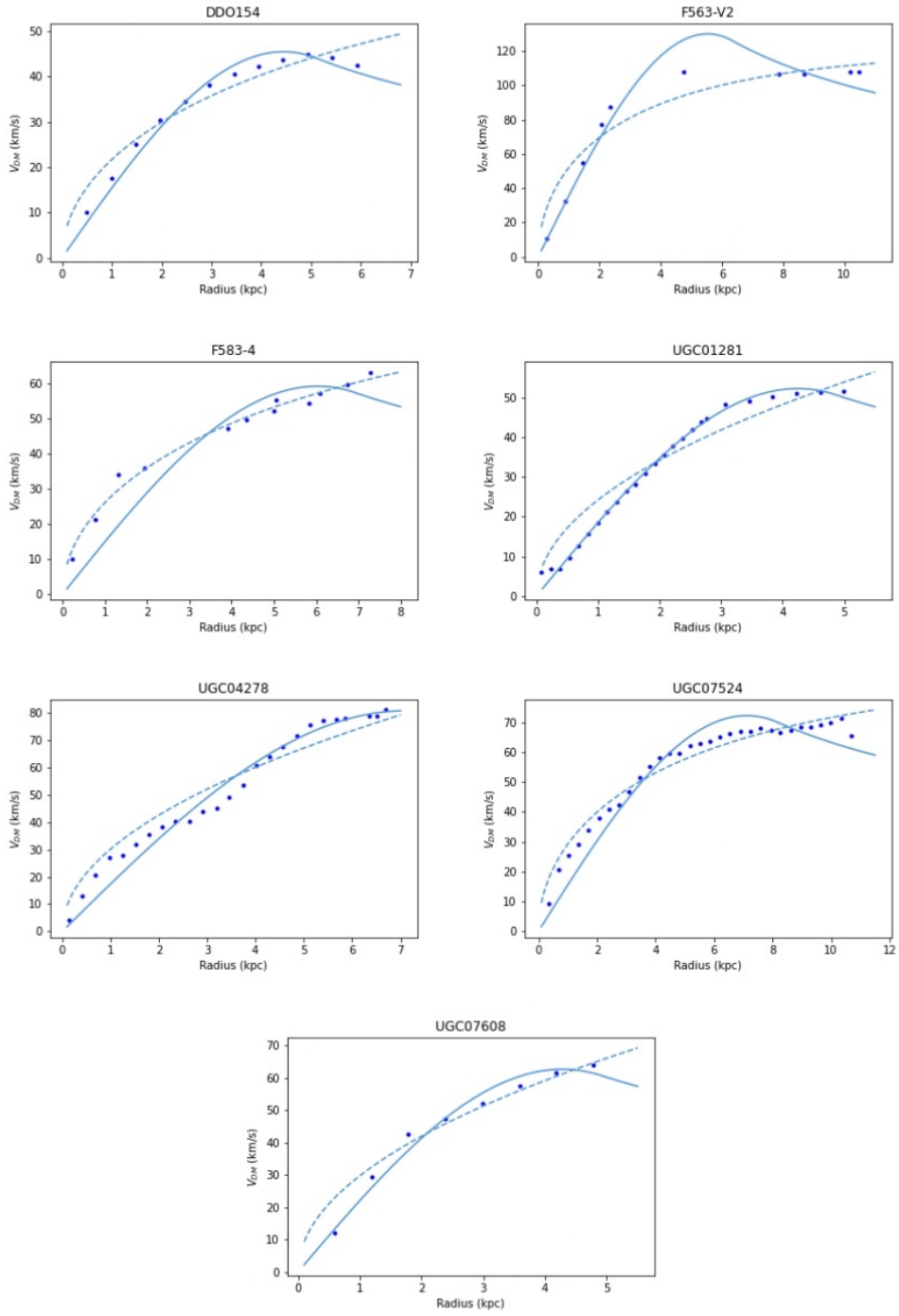

Figure 7: Comparison of the velocity of the rotation curves obtain with the BEC dark matter model (solid curve), of the velocity fits obtained with the NFW density profile (dashed curve), and of the observed rotational curves of eight galaxies

8.2 Density profile

The corresponding density profiles of the dark matter halos for the BEC and NFW model can be seen in Figures 8 and 9, respectively. As can be seen, in the density profile of the BEC model there is no singularity, there is a finite central density, which does not occur in the density profile of NFW, where there is a singularity or cusp in the center of the galaxy, for $r \to 0$. This is the cusp-core problem that has been introduced in previous sections, and we see that with the BEC model this challenge is solved. The mass distribution of the gravitationally bounded condensate decreases slowly as a function of r, with most of the matter concentrated in a core-like region. Another relevant difference is that, although the NFW profile tends faster to zero than the BEC profile, the latter does not have a well-defined radius, whereas the BEC profile predicts a finite and well-defined radius for the dark matter distribution, whose density is zero on a surface defined by radius R. Thus the BEC model predicts that the dark matter distribution may be affected so that the central cusps predicted by the cosmological simulations are flattened, resulting in dark matter halos more similar to those found observationally.

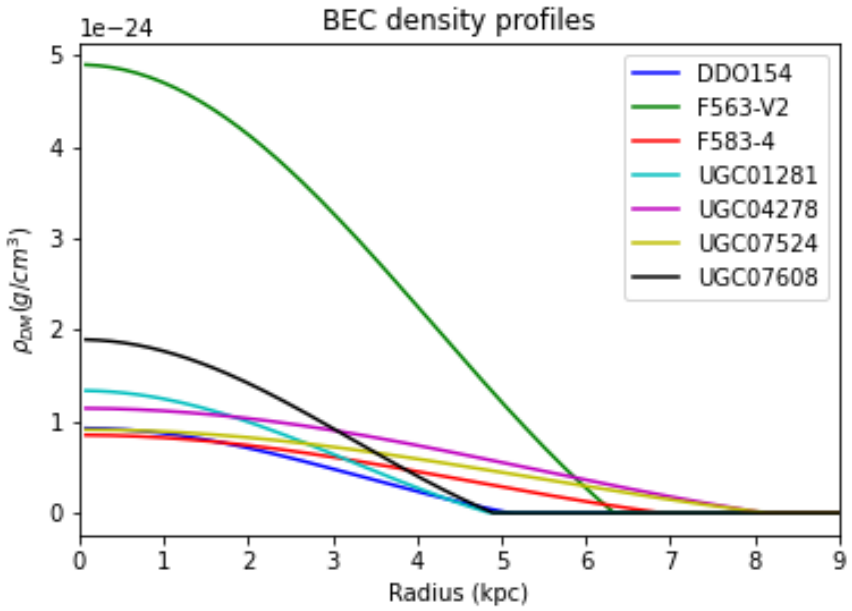

Figure 8: BEC dark matter density profiles for the galaxies used in this study.

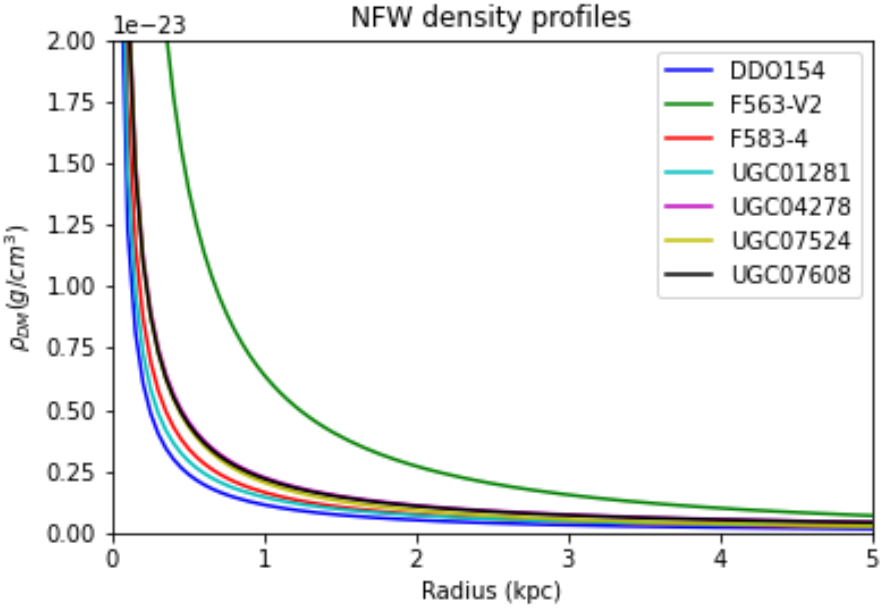

Figure 9: NFW dark matter density profiles for the galaxies used in this study.

9 Conclusion

En esta última sección se comentará lo prometedor que es el modélo usado, pero también se remarcará los problemas que este presenta

---

As can be seen in section 8, the results obtained with the model based on Bose-Einstein condensates fit very well to the observational data extracted from the SPARC database. This model can even solve the famous cusp-core problem as previously discussed, however, this model is far from being a good model. In this work we have obtained different values for the central density of the condensate $\rho_{DM}^{(c)}$and the radius R for each galaxy. This shows us that the model, although a very good first approximation, cannot be right. R, as shown in Eq.(65), depends on the ratio a_s/m^3, where a_s is the s-wave scattering length and m is the individual particle mass, so that different R and $\rho_{DM}^{(c)}$ for each galaxy implies that the dark matter halo condensates are different for each galaxy. This indicates that the model cannot be entirely correct.

Regardless of the fact that the model presented is only a first approximation, this work shows that this type of approximation is one of the best ways to find solutions to the problems presented by dark matter.

References

[1] Gianfranco Bertone and Dan Hooper, History of dark matter, Review of Modern Physics, 90, 045002 (2018).

[2] K.Freese, Review of observational evidence for dark matter in the universe and in upcoming searches for dark stars, in Dark Energy and Dark Matter: Observations, Experiments and Theories, E. Peconal, T.Buchert, Ph. Di Stefano and Y. Copin (eds), EAS Publications Series 36, 113 (2009).

[3] J. P. Ostriker, E. Choi, A. Chow and K. Guha, Mind the gap: is the too big to fail problem resolved?, 885, 97 (2019).

[4] Elisa G. M. Ferreira, MPA Lectures - Alternatives Models of Dark Matter: Ultra Light fields (2019).

[5] F. Dalfovo, S. Giorgini, L. P. Pitaevskii, and S. Stringari, Theory of Bose-Einstein condensation in trapped gases, Rev. Mod. Phys. 71, 463 (1999).

[6] J. Rogel-Salazar, The Gross–Pitaevskii equation and Bose–Einstein condensates, European journal of physics, 34, 247 (2013).

[7] Pierre-Henri Chavanis, Dissipative self-gravitating Bose-Einstein condensates with arbitrary nonlinearity as a model of dark matter halos, 2016.

[8] B.H. Bransden and Charles Joachain, Quantum Mechanics, Prentice Hall, 01 (2000). ISBN 0582-35691-1.

[9] C.G.Böhmer and T.Harko. Can dark matter be a Bose–Einstein condensate?, JCAP06, 025 (2007).

[10] T.Harko.Bose-Einstein condensation of dark matter solves the core/cusp problem, JCAP05, 022 (2011).

[11] F. Lelli, S. S. McGaugh, and J. M. Schombert, SPARC: Mass models for 175 disk galaxies with spitzer photometry and accurate rotation curves, The Astronomical Journal,152(6):157 (2016). URL: **http://dx.doi.org/10.3847/0004-6256/152/6/157**.